Comparison of Micropore Distribution in Cell Walls of Softwood and Hardwood Xylem[1]

Lloyd A. Donaldson,[a,2,3] Mathew Cairns,[b] and Stefan J. Hill[a]

[a]Scion, Rotorua 3010, New Zealand

[b]Victoria University of Wellington, Wellington 6140, New Zealand

ORCID IDs: 0000-0002-3845-4177 (L.A.D.); 0000-0001-9096-5057 (M.C.); 0000-0003-4452-9152 (S.J.H.)

The porosity of wood cell walls is of interest for both understanding xylem functionality and from a wood materials perspective. The movement of water in xylem generally occurs through the macroporous networks formed in softwood by bordered pits and in hardwood by the intervessel pits and open conduits created by vessels and perforation plates. In some situations, such as cavitated xylem, water can only move through the micropores that occur in lignified tracheid and fiber cell walls; however, these micropore networks are poorly understood. Here, we used molecular microscopy analysis of radiata pine (*Pinus radiata*) and red beech (*Nothofagus fusca*) to determine the distribution of micropores in the secondary walls and middle lamellae of tracheids and fibers in relation to cell wall composition. Using two different types of probe, we identified a greater porosity of secondary cell walls and a reduced porosity of the middle lamella. Areas of reduced porosity were observed in the outer regions of the secondary cell wall of both tracheids and fibers that appear unrelated to lignification or the distribution of cellulose, mannan, and xylan. Hardwood fiber cell walls were less lignified than those of softwood tracheids and showed greater accessibility to porosity probes. Vessel cell walls were comparable to those of fibers in terms of both porosity and lignification. Lignification is probably the primary determinant of cell wall porosity in xylem. The highly lignified middle lamella, and lumen surface, act as a barrier to probe movement and, therefore, water movement in both softwood and hardwood.

Xylem cells in conifers and flowering plants have specialized secondary cell walls that facilitate water conduction from roots to leaves and provide mechanical support for the stem and branches (Hacke and Sperry, 2001). These cell walls are composed of cellulose, hemicellulose, and lignin, forming a complex nanocomposite (Hill et al., 2009). One aspect of this structure that is poorly understood is its porosity. Micropores are pores less than 2 nm in size, whereas mesopores range in size from 2 to 50 nm (Rouquerol et al., 1994). In the sapwood of living trees, xylem cell walls usually are saturated with water, which occupies the micropores within the cell wall. In wet cell walls, micropores constitute the majority of water-accessible pathways. Specialized areas of the cell wall known as pit membranes, which are involved in regulating water movement between cells, may contain both micropores and mesopores. The bordered pits of softwoods, for example, contain a margo, which is mesoporous, and a torus that is microporous (Choat et al., 2008). Mesopores also may originate from cell wall checking, as a result of timber drying, and the subsequent shrinkage of cell walls, as a result of wood decay, or as a result of chemical extraction during industrial processing, such as delignification in paper pulp production, for example (Stone, 1964; Skaar, 1988). Macropores (greater than 50 nm) in xylem are represented by cell lumens (Skaar, 1988; Hacke and Sperry, 2001) and mostly form the water-conducting system of the plant.

Micropores are effectively closed in dry cell walls, making their direct observation by electron microscopy impractical for native lignified cell walls (Davies, 1968; Xu et al., 2007). Treatments such as delignification or fungal degradation can enlarge micropores, thus allowing their direct observation. Most of the studies on cell wall mesopores have been performed using such altered samples (Davies, 1968; Donaldson, 1988; Blanchette et al., 1997; Hill and Papadopoulos, 2001; Xu et al., 2007; Kojiro et al., 2010; Borrega and Kärenlampi, 2011; Ciesielski et al., 2013; Pu et al., 2013; Yin et al., 2017). It is possible to measure the size distribution of all pores by physicochemical methods, such as porosimetry, gas adsorption, or freezing point depression; however, these methods provide only a bulk measurement of pore size range, including that for both micropores and mesopores (Hill and Papadopoulos, 2001; Grigsby et al., 2013).

The distribution of micropores in xylem cell walls is of interest from both a biological and a materials perspective. These minor apoplastic pathways are

[1]This research was funded by the New Zealand Ministry of Business, Innovation, and Employment, via the Strategic Science Investment Fund.

[2]Author for contact: lloyd.donaldson@scionresearch.com.

[3]Senior author.

The author responsible for distribution of materials integral to the findings presented in this article in accordance with the policy described in the Instructions for Authors (www.plantphysiol.org) is: Lloyd A. Donaldson (lloyd.donaldson@scionresearch.com).

L.A.D. conceived the project and performed the microscopy; S.J.H. performed the molecular modeling; M.C. performed the dynamic light-scattering measurements; L.A.D. wrote the article with contributions of all the authors; all authors read and approved the final article.

www.plantphysiol.org/cgi/doi/10.1104/pp.18.00883

Table 1. Molecular dimensions for quenching agents and rhodamine

NPGU, 4-Nitrophenyl β-D-glucuronide; NPGP, 4-nitrophenyl α-D-glucopyranoside; NPXT, 4-nitrophenyl β-D-xylotrioside; NPMP, *p*-nitrophenyl α-D-maltopentaoside; NPMH, 4-nitrophenyl α-D-maltohexaoside.

Probe	No. of Hexose Units	M_r	Stokes Radius	Calculated Molecular Volume	Length	Width	Aspect Ratio
		g mol^{-1}	*Å*	*Å*^{3}	*Å*		
NPGU	1	301.2	5	224	11	4	2.75
NPGP	1	301.2	5	222	10	7	1.43
NPXT	3	535.4	7	415	20	8	2.50
NPMP	5	949.8	10	770	19	14	1.36
NPMH	6	1,111.9	10	924	35	6	5.83
Rhodamine	–	442.6	4	367	16	8	2.00

important during heartwood formation, where cell walls may replace their water with gums and extractives involved in defense responses, resulting in reduced permeability (Yin et al., 2015). In aspirated xylem, cell wall micropores can provide an alternative route for water movement and potentially allow for the refilling of conduits (Brodersen and McElrone, 2013; Ryu et al., 2016). The cuticle and Casparian strips in other tissues also are examples of how plants use porosity to control water and solute movement (Wu et al., 2005; Schönherr, 2006).

From a materials point of view, cell wall micropores provide pathways for water loss during timber drying and for infiltration with chemicals during chemical modification and timber preservative treatments (Skaar, 1988). The size and range of micropores within cell walls also determine the accessibility to enzymes and, thus, have a direct impact on the utilization of cellulosic biomass for biofuel applications and on wood decay (Blanchette et al., 1997; Hill et al., 2005; Chundawat et al., 2011; Pu et al., 2013; Donaldson and Vaidya, 2017). Therefore, studies that provide fundamental knowledge of these porous networks are of significant interest.

The spatial distribution of micropores in native wet cell walls of different cell types and in different cell wall regions has not been investigated (Yin et al., 2015). Methods for detecting and measuring micropores in wood cell walls using fluorescence microscopy have been developed recently (Donaldson et al., 2015). In this study, micropore distribution in wood cell walls was determined using two approaches, one involving infiltration with quenching agents that reduce the fluorescence of lignin adjacent to the pores and a second method involving infiltration with a fluorescent dye in combination with Förster resonance energy transfer (FRET). The accessibility of the secondary cell wall and middle lamella to both probes was compared for the typical softwood radiata pine (*Pinus radiata*) and the typical hardwood red beech (*Nothofagus fusca*), thus providing insight into the nature of micropores in lignified cell walls.

RESULTS

Cell wall porosity is assessed by measuring the infiltration of pores with two different types of solute probe. Nitrophenol carbohydrates covering a range of different M_r values are detected by their effect on lignin autofluorescence. The amount of infiltration using dilute solutions is detected by measuring the reduction in brightness (quenching) of cell walls compared with a water-treated control. Alternatively, infiltration with rhodamine dye is detected both directly by its red fluorescence and quantitatively by measuring the FRET interaction between dye molecules and lignin. FRET interaction occurs when the donor (lignin) and acceptor (rhodamine) molecules are in close proximity (less than 10 nm). The acceptor photobleaching technique is used where the acceptor molecules are bleached by high-intensity laser irradiation, and the resulting increased donor fluorescence within the irradiated area is measured and compared with the intensity before bleaching.

Molecular Characteristics of Probes

Dynamic light-scattering measurements and molecular dynamics calculations were used to estimate the size of molecular probes so that this could be related to pore size. Measurements show that nitrophenol carbohydrates generally increase in size with M_r but remain largely linear in shape (Table 1; Donaldson et al., 2015). For these probes, infiltration may be limited by increasing M_r, which impacts the ability of the molecule to bend around corners. In comparison, rhodamine is a disk-shaped molecule (Table 1), which may account for the greater amount of differential rhodamine infiltration in different cell wall regions compared with that of quenching probes of similar M_r. The tortuosity of micropores and details of their shape relative to the probe molecule are not known. Both types of probe probably form larger micelles in solution, but it was assumed that such larger structures would be excluded from micropores because of their size and, hence, played no role in microscopy measurements.

Characterization of Porosity by Quenching

Lignin autofluorescence was found to be brighter in pine than in beech, with an average brightness of 1,240 ± 23 gray levels for pine compared with 922 ± 21 for

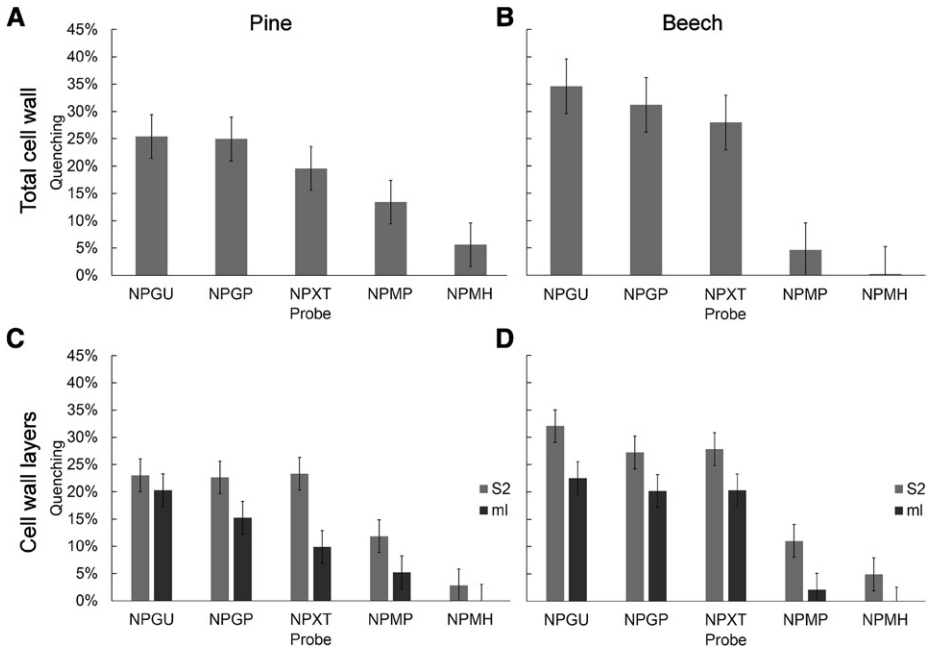

Figure 1. Nitrophenyl quenching measurements for pine and beech. A and B, Comparison of total cell wall quenching for pine (A) and beech (B). C and D, Comparison of middle lamella (ml) and secondary wall (S2) quenching in pine (C) and beech (D). Error bars represent the 95% confidence interval based on 10 independent measurements. NPGU = 1 hexose unit, NPGP = 1 hexose unit, NPXT = 3 hexose units, NPMP = 5 hexose units, and NPMH = 6 hexose units.

beech under constant gain, based on 40 replicate measurements. The ratio of middle lamella fluorescence to secondary wall fluorescence was 2 in pine and 2.5 in beech, whereas the brightness of the secondary wall in pine (1,078 ± 19) was higher than in beech (793 ± 17). This difference suggests a less lignified secondary wall in beech fibers compared with that in pine tracheids. Beech vessels were indistinguishable from fibers at UV excitation. Quenching measurements for vessel walls at UV excitation were impractical due to the very thin vessel cell wall; however, based on a visual comparison, vessel and fiber cell walls remained comparable in brightness after quenching.

The overall quenching effect for probes covering a range of M_r values was less in pine than that in beech (Fig. 1, A and B), indicating a greater interaction of quenching agents with lignin in beech and, hence, a greater porosity. For the two monosaccharide quenching agents NPGP and NPGU, which have the same M_r but slightly different chemical structures, overall quenching measurements were the same (Fig. 1A). However, for wall layer measurements (Fig. 1, C and D), pine showed a significant difference between NPGP and NPGU in the middle lamella region, whereas beech showed a significant difference in the S2 region. In both cases, the difference was small ($P = 0.037$, F test). This suggests that differences in the chemical structures of probes may have a relatively small effect compared with that of M_r, but their impact can still be detected. There may be ways of enhancing this difference, for example by using probes at a higher concentration to achieve greater levels of quenching.

As expected, quenching measurements for pine were reduced with increasing probe M_r, but a significant, although small, amount of quenching still was observed with the 6-hexose probe. By contrast, beech showed a gradual reduction in quenching with increasing probe M_r, with a sudden reduction to negligible levels for the 5- and 6-hexose probes. This indicates that pores are smaller in beech fiber cell walls compared with that of pine tracheids and, together with the overall greater quenching levels in beech, implies a greater cell wall porosity consisting of more frequent but smaller pores in beech fibers compared with that in pine tracheids.

For both pine and beech, the secondary wall was quenched to a greater extent than the middle lamella, indicating greater porosity in the secondary wall than in the middle lamella (Fig. 1, C and D). For the secondary wall in both pine and beech, quenching showed little change until the 5-hexose probe, suggesting that these pores are of a similar size range in both species. Beech secondary walls showed a higher quenching level for the smaller probes, again indicating that beech secondary walls are more porous than those of pine (Fig. 1D).

The amount of quenching was less in the middle lamella than in the secondary wall for both species, indicating that the middle lamella is less porous than the secondary wall (Fig. 1, C and D). In pine, the middle lamella showed a gradual decline in quenching with increasing probe M_r, whereas the middle lamella in

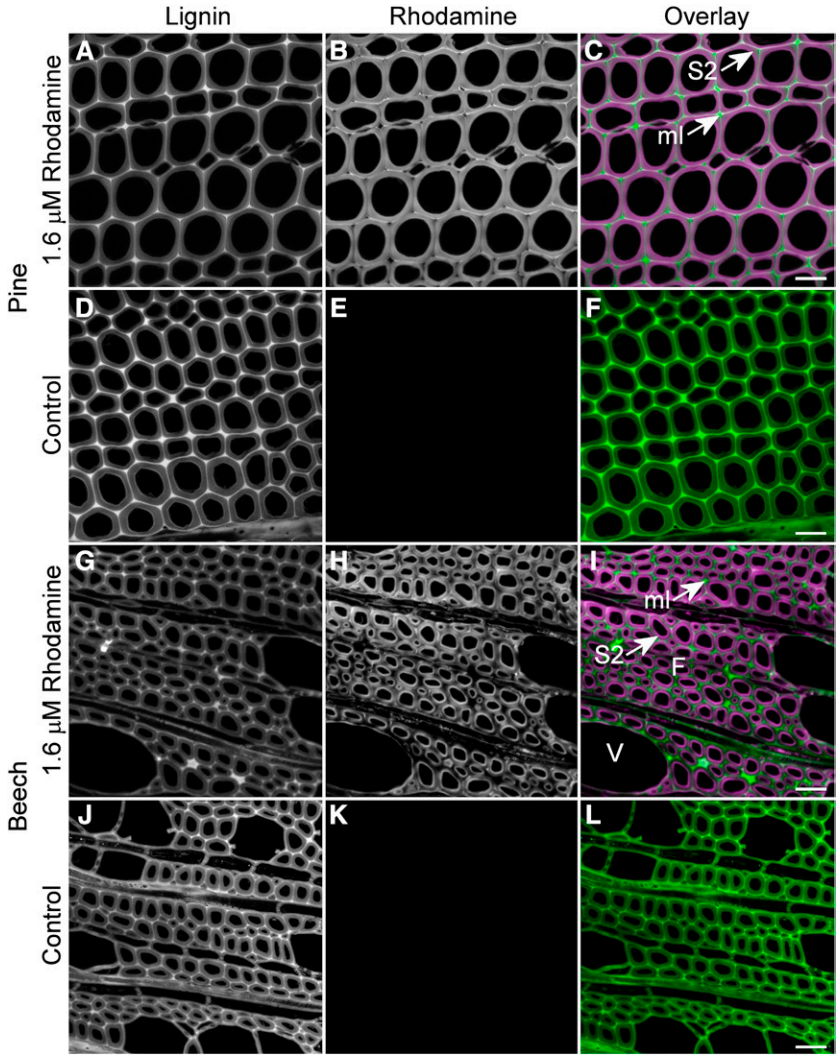

Figure 2. Comparison of rhodamine infiltration between pine and beech. A to C, Infiltration of pine sections with rhodamine occurs in the secondary wall (S2) with exclusion in the more highly lignified middle lamella (ml) and in the secondary wall at the cell corners. The overlay image shows lignin in green and rhodamine in magenta. D to F, Control images of pine sections with no rhodamine confirm the absence of a lignin signal in the rhodamine channel at a fixed gain. The lignin channel is somewhat brighter in the absence of rhodamine due to quenching resulting from FRET interaction. G to I, Infiltration of beech sections with rhodamine occurs in the S2 with exclusion from the middle lamella and outer secondary wall. Vessel (V) cell walls seem to be less infiltrated than adjacent fibers (F). J to L, Control images of beech sections with no rhodamine confirm the absence of lignin signal in the rhodamine channel at a fixed gain. The lignin channel is brighter in the absence of rhodamine due to quenching resulting from FRET interaction when rhodamine is present. Bars = 30 μm.

beech showed the same abrupt transition as that for the secondary wall, thus suggesting a narrower distribution of pore size in beech compared with pine. The middle lamella showed less quenching for pine than for beech, confirming that both wall regions are less porous in pine than in beech.

Characterization of Porosity by Rhodamine Infiltration and FRET

Treatment and infiltration with rhodamine showed two types of interaction with wood sections (Figs. 2 and 3). At the surface of the section, rhodamine bound to the cell wall, forming an intensely fluorescent layer. Below the surface, rhodamine penetrated the cell wall for a short distance of about 15 μm. Further diffusion presumably was limited by clogging of pores due to the binding interaction between rhodamine and the cell wall. Characteristically, quenching probes can easily be washed out of the section within a few minutes, whereas rhodamine requires long periods of washing (more than 24 h) to remove it from the cell wall. Rhodamine, therefore, shows a binding interaction with the cell wall, whereas nitrophenyl-labeled carbohydrates do not show binding behavior.

By focusing on the cell wall 5 to 10 μm below the surface of the section with confocal microscopy, it was possible to visualize the differential infiltration of cell wall regions by rhodamine solution after a 1-h incubation. Rhodamine penetrated the inner part of the secondary cell wall in both pine tracheids and beech fibers (Figs. 2 and 3). However, in pine, rhodamine was partially excluded from the outer secondary wall predominantly near the cell corners and was excluded from the middle lamella region (Figs. 2 and 3). The S1 layer in pine showed strong infiltration with rhodamine (Fig. 3A), suggesting that it is highly porous compared with other regions. In beech fibers, rhodamine was excluded from the outer secondary wall and middle lamella uniformly around the circumference of the cell rather than localized to the cell corners, as observed with pine (Figs. 2 and 3). These results confirm those determined

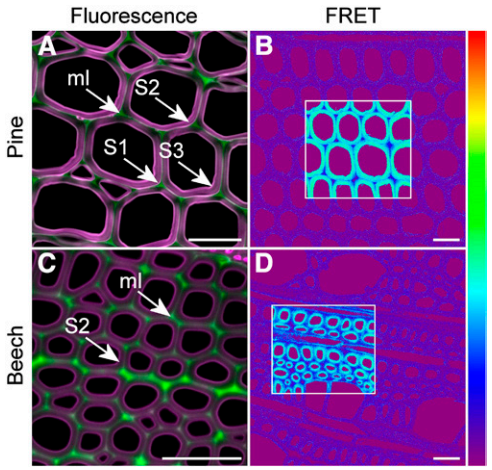

Figure 3. Comparison of rhodamine infiltration in sections of pine and beech. A, Fluorescence overlay image with lignin displayed as green and rhodamine as magenta. Rhodamine infiltration of pine sections is greater in the S1 and S3 layers of the secondary wall. B, FRET efficiency image. Rhodamine-infiltrated sections show high levels of FRET between lignin (donor) and rhodamine (acceptor) in regions where acceptor photobleaching was performed (boxed). C, Fluorescence overlay image with lignin displayed as green and rhodamine as magenta. Rhodamine is excluded from the outer secondary wall and middle lamella (ml) in beech fibers in a pattern slightly different from that of pine and with no indication of increased infiltration in the S1 and S3 layers. D, FRET efficiency image. FRET efficiency in the secondary wall of beech fibers is slightly lower compared with that of pine tracheids. The color scale represents 0% to 100% FRET efficiency. Bars = 30 µm.

by quenching, indicating that the middle lamella has fewer and/or smaller pores than the secondary wall in both species.

To confirm the absence of rhodamine in the middle lamella, FRET interactions were measured across the cell wall using acceptor photobleaching. Strong FRET interactions were observed between rhodamine and lignin in the secondary wall with FRET efficiencies of 30% to 40% (Table 2). By contrast, FRET interactions were weak or not observed in the middle lamella, confirming that rhodamine is excluded from this region (Fig. 3, B and D). FRET interactions were somewhat less when measured under dry conditions (in immersion oil) compared with that under wet conditions (in 50% [v/v] glycerol; Table 2). In beech, vessel cell walls showed slightly less infiltration with rhodamine than that in adjacent fiber walls (Fig. 2I), but FRET interactions were similar to those in fiber cell walls (Fig. 3D).

Rhodamine also was used to determine the diffusion pathway into the cell wall using treated blocks, as compared with transverse sections, where there is free access to all regions of the cell wall (Fig. 4). Longitudinal sections of such blocks confirmed that rhodamine diffuses into the cell wall from the transverse cut end only for a distance of about 15 µm, confirming observations for treatments on transverse sections. Behind this zone, rhodamine can only enter the cell wall from the lumen surface. Transverse sections from this region showed an intense layer of rhodamine adjacent to the lumen surface but little or no infiltration of the cell wall and no FRET interaction. This confirms that the lumen surface, which corresponds to the S3 layer of the cell wall, is relatively impermeable compared with the S2 region. In beech, there was an indication of different behavior between vessels and fibers, possibly due to a difference in the hydrophobicity of the lumen surface (Fig. 4K). Diffusion of rhodamine from cut longitudinal surfaces was much greater (60 µm compared with 15 µm) than that from the cut transverse surface, suggesting that there is some directional aspect to cell wall porosity. It is quite likely that some pores may be aligned with the cellulose microfibril orientation and lamellar structure of the cell wall (Fahlén and Salmén, 2005).

Chemical Composition

The analysis shown in Table 3 is based on the generally accepted method for the determination of carbohydrate and lignin (Klason) amounts (Pettersen, 1991). However, the results have not been corrected for any pseudolignin or other insolubles that may have formed during sample preparation prior to analysis (Kobayashi et al., 1960; Sannigrahi et al., 2011). Beech wood had less acid insolubles (Klason lignin) than pine wood, although it had a higher content of acid solubles. This supports the conclusion from fluorescence intensity measurements indicating less lignification in secondary walls of beech fibers compared with pine tracheids. As expected, beech carbohydrates were richer in xylan whereas pine carbohydrates were richer in mannan (Table 3). The location of extractives in beech

Table 2. FRET measurements using lignin as donor and rhodamine as acceptor

Values are means based on five replicate fields of view per treatment ± the 95% confidence interval.

Sample Type	Mountant	Pine	Beech
Sections			
Wet + rhodamine	Glycerol	43.5% ± 2.3%	40.8% ± 2.3%
Wet + rhodamine	Immersion oil	34.7% ± 2.3%	21.9% ± 2.3%
Wet control	Glycerol	0.5% ± 0.5%	0.4% ± 0.5%
Wet control	Immersion oil	1.0% ± 0.5%	0.0% ± 0.5%
Blocks			
Wet + rhodamine	Immersion oil	0.1% ± 0.5%	0.5% ± 0.5%
Dry + rhodamine	Immersion oil	0.0% ± 0.5%	0.9% ± 0.5%

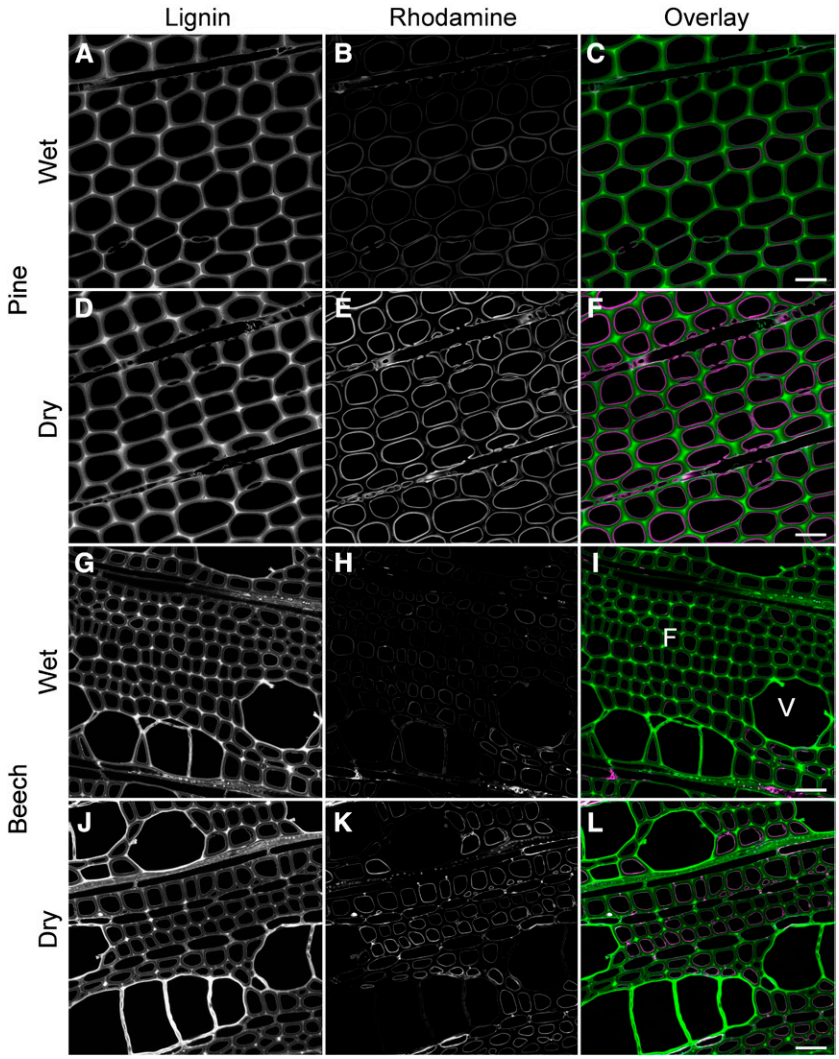

Figure 4. En-bloc rhodamine infiltration performed on wet or air-dried blocks. A to C, Rhodamine infiltration in transverse sections cut from pine blocks that were wet prior to rhodamine treatment. Rhodamine is restricted to the lumen surface, indicating a barrier to infiltration. D to F, Rhodamine infiltration in transverse sections of pine blocks that were air dried prior to rhodamine treatment. G to I, Rhodamine infiltration in transverse sections cut from beech blocks that were wet prior to rhodamine treatment. J to L, Rhodamine infiltration in transverse sections of beech blocks that were air dried prior to rhodamine treatment. Fibers (F) accumulated more rhodamine on the lumen surface than adjacent vessels (V). Bars = 30 µm.

sapwood was mostly in the ray tissue, as determined by fluorescence. The extent to which extractives also were present in the fiber cell walls is not known, so an influence of extractives on porosity measurements is difficult to interpret.

The observed difference in lignin content between beech and pine agrees with their difference in porosity, in that beech had a larger number of smaller pores than pine and also was less lignified. This role of lignin also is supported by the observed reduced porosity of the highly lignified middle lamella in both species (Donaldson, 2001) and by the exclusion of rhodamine by the highly lignified S3 layer in en-bloc treatments.

Table 3. Sample composition measured as percentage (w/w) of extracted oven-dried sample

Average values are based on two replicates.

Extractives	Lignin and Other Insolubles		Neutral Carbohydrates as Anhydrosugars					Total
	Acid Insoluble (Klason)	Acid Soluble	Arabinosyl Units	Galactosyl Units	Glucosyl Units	Xylosyl Units	Mannosyl Units	
Pine								
0.64	28.74	0.61	1.55	1.60	47.86	5.12	10.60	96.08
0.63	27.78	0.57	1.28	1.68	49.10	5.22	11.01	96.63
0.63	28.26	0.59	1.42	1.64	48.48	5.17	10.80	96.36
Beech								
8.98	21.67	4.46	0.34	0.85	39.81	20.24	2.62	90.00
9.08	21.71	4.98	0.32	0.79	41.24	21.19	2.69	92.92
9.03	21.69	4.72	0.33	0.82	40.52	20.71	2.66	91.46

The difference in hemicellulose composition is typical of the generic differences between hardwoods and softwoods (Scheller and Ulvskov, 2010). Xylan amounts may influence accessibility due to the formation of carbohydrate-lignin linkages (Sorieul et al., 2016).

Histochemistry

Interference microscopy was used to estimate the lignin concentration of cell wall layers by determining the refractive index of cell walls compared with the refractive index of lignin and carbohydrate components assuming a linear relationship with lignin concentration.

Measurements of lignin concentration within cell wall layers showed that the S2 region of red beech fibers was slightly less lignified than in pine tracheids (18% versus 21%; Fig. 5), confirming observations made using fluorescence (Fig. 2, G and J) and chemical (Table 3) analyses. Vessel secondary walls were lignified to the same extent as were fibers in red beech. The middle lamella in both wood types was more lignified, with about 80% (v/v) lignin.

Mannans and xylans were localized using fluorescently labeled antibodies. Mannans were localized within the secondary wall of pine tracheids and beech fibers and tended to show slightly increased amounts at the S1 layer in pine but were largely absent from the S1 layer in beech (Fig. 6, C and D). Beech vessels showed negligible mannan labeling compared with fibers, similar to the results reported for Arabidopsis (*Arabidopsis thaliana*) and poplar (*Populus* spp.; Kim and Daniel, 2012a, 2012b). Labeling of mannan epitopes in beech was reduced significantly compared with pine (Fig. 6D). Xylans were distributed in both primary and secondary walls of tracheids, fibers, and vessels but often tended to be less abundant in primary walls of some cells in beech (Fig. 6, E and F).

Analysis of lignin distribution by acriflavin staining was in agreement with the results of interference microscopy and autofluorescence, showing low lignification in secondary walls and high lignification in the middle lamella (Fig. 6, A and B). High lignification in the S3 layer at the lumen surface was more pronounced for pine tracheids than for beech fibers.

Tracheids, fibers, and vessels all had secondary walls with a typical three-layered arrangement; however, the three layers in vessels were approximately the same thickness, whereas those in tracheids and fibers had thick S2 layers (Fig. 6, G and H). Vessels also had very thin cell walls compared with fibers, as reported for other species by Kishi et al. (1977).

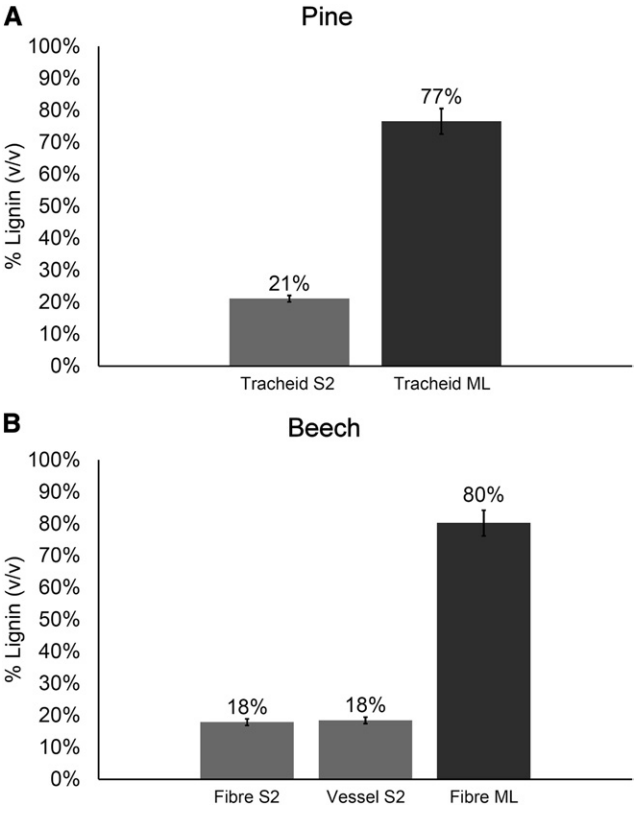

Figure 5. Comparison of lignification in pine and beech. Measurements of percentage lignin (v/v) in pine (A) and beech (B) tissues by interference microscopy are shown. Measurements were based on 10 replicates. Error bars show the 95% confidence interval. ML, Middle lamella.

DISCUSSION

Using nitrophenyl carbohydrate probes, we investigated the micropore distribution in native cell walls and demonstrated differences between a typical softwood and a typical hardwood. We extended this work using rhodamine as a probe of similar M_r but with a more globular shape and with greater binding interactions with cell wall components to demonstrate variations in porosity across the cell wall. Differences in the behavior of rhodamine and nitrophenyl probes revealed a barrier at the lumen surface in both wood types that can be penetrated by NPGP (Donaldson et al., 2015) but not by rhodamine (Fig. 4).

Factors that influence the infiltration of cell walls by small molecules include molecular mass, the charge of the solute, pore size, interconnectedness, restricted areas, and surface characteristics (Wu et al., 2009). In this investigation, we were able to detect small but significant differences in infiltration between the two smallest quenching probes, namely NPGP and NPGU, which have the same M_r but differ slightly in chemical structure, with a terminal hydroxyl on NPGU and a terminal carboxyl on NPGP. The wide range of nitrophenyl-based molecules of various shapes and charge available may allow further investigation of different pore characteristics in future studies.

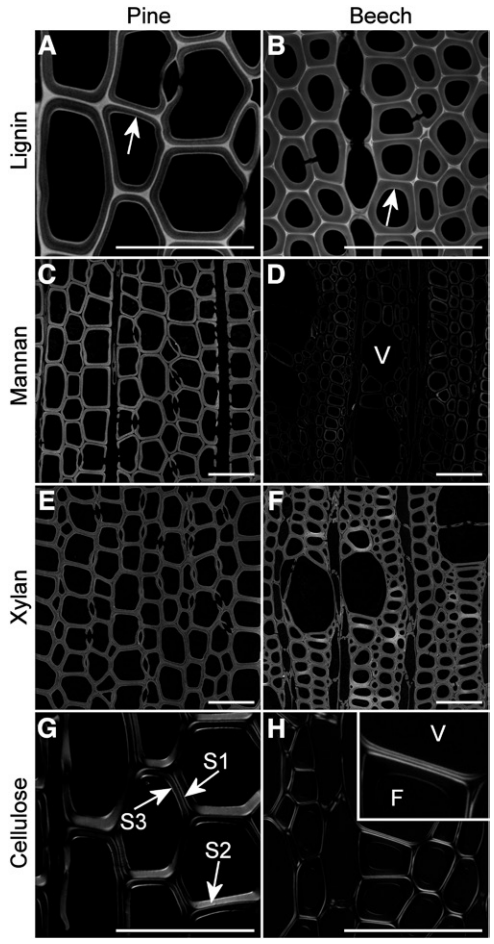

Figure 6. Histochemical analysis of major cell wall components in radiata pine and red beech. A and B, Lignin distribution in pine (A) and beech (B) represented by acriflavin staining. Arrows indicate greater lignification in the S3 layer. C to F, Mannan and xylan distribution in pine (C and E) and beech (D and F) represented by LM21 and LM11 immunolabeling, respectively. Each image was acquired at the same gain, so relative intensity reflects relative amounts of the epitope. Vessels (V) contain little or no mannan labeling compared with fibers. G and H, Cellulose distribution in pine (G) and beech (H) represented by polarized light images. Vessel (V) cell walls show a very thin S2 compared with that in fiber (F) cell walls, with comparable thickness of S1, S2, and S3 in vessels. Bars = 50 μm.

In our previous study (Donaldson et al., 2015), we compared the porosity of supercritical CO_2-dewatered wood, where water is removed from cell lumens but the cell wall remains saturated, with that of kiln-dried wood, where the cell walls were dried at 90°C. This comparison indicated that pores were distributed unevenly in the secondary cell wall, with limited accessibility in regions near the cell corners. This uneven distribution was more apparent in kiln-dried wood, probably due to the irreversible closure of some micropores as a result of drying (Stone, 1964; Davies, 1968). In this study, we have confirmed that these less accessible regions also exist in never-dried pine wood using rhodamine as a probe. In red beech fibers, a similar region of reduced accessibility was observed in the outer secondary wall with less localization to the cell corners (Fig. 3). The reasons for the reduced accessibility in the outer secondary wall are not apparent: there is no obvious relationship to lignin or carbohydrate distribution (Fig. 6). Imaging and FRET measurements on wet (glycerol) or dry (immersion oil) sections (Table 2) indicated that this reduced accessibility is not related to the drying of cell walls. These areas are not known to have different composition or ultrastructure. Variations in the porosity of the secondary wall have not been observed in studies involving mechanically or chemically altered cell walls (Fahlén and Salmén, 2002; Kielmann et al., 2014).

We also confirmed that the middle lamella region is much less accessible to solutes in both wood types using both quenching probes and rhodamine. Other studies have indicated that the middle lamella is less porous than the secondary wall (Donaldson et al., 2014). A less porous middle lamella could potentially limit the movement of water and solutes between adjacent cells and at least in tracheids and vessels, which would reduce the leakiness of water conduits while allowing the inner part of the cell wall to remain saturated with water and, thus, remain mechanically flexible (Meng et al., 2015).

Previous comparisons of en-bloc infiltration compared with infiltration of sections have indicated that thin sections are more accessible than blocks, as, for the latter, probes must enter the cell wall via the lumen surface (Donaldson et al., 2015). In both pine tracheids and beech fibers, the lumen surface consists of the S3 layer of the secondary wall, which is more lignified than the adjacent S2 layer and perhaps more so in pine than in beech (Fig. 6, A and B; Donaldson, 1987; Donaldson and Knox, 2012). Thus, the observation that this cell wall layer appears to limit (quenching probes) or prevent (rhodamine) infiltration agrees with the known increased deposition of matrix materials and hydrophobicity at the lumen surface (Zwieniecki and Holbrook, 2000; McCully et al., 2014). However, there is another pathway for cell wall infiltration associated with the lumen at bordered pits in pine tracheids. At the margin of the pit border, the S1 layer is exposed to the lumen. We found that the S1 region of cell walls on treated sections showed high accessibility to rhodamine, suggesting greater porosity that is most likely associated with reduced lignification in this region (Donaldson, 1995). Red beech fibers did not show increased accessibility of the S1 region on rhodamine-treated sections. We did not observe infiltration of the S1 region adjacent to pits in either species when samples were infiltrated en bloc, indicating that this infiltration route is not accessible to rhodamine.

Since micropores are too small to image directly, we can only infer their shape characteristics by varying the shape of the probe. The carbohydrate quenching probes are linear molecules (Table 1) and, hence, will tend to be excluded if pores are short or tortuous.

If we assume that pore diameter is similar to hydrodynamic radius, then quenching probes will tend to be excluded if they have insufficient flexibility to negotiate bends. In the case of rhodamine, this molecule is disc shaped (Table 1), so exclusion may depend more closely on pore diameter irrespective of tortuosity. However, a further complicating factor is that, in contrast to quenching probes, which are nonbinding, rhodamine binds weakly with the cell wall. Binding probes will tend to clog the pores, thus restricting accessibility. This would explain why en-bloc infiltration with rhodamine is much less effective than with quenching probes (Donaldson et al., 2015), even though they have a similar hydrodynamic radius (Table 1).

A number of studies have examined pore shape in dried and in modified wood cell walls. Both earlywood and latewood tracheid cell walls in high-temperature-dried Norway spruce (*Picea abies*) contained a similar amount of micropores (Borrega and Kärenlampi, 2011). Micropores have been described as slit-like spaces between adjacent lamellae (Stone and Scallan, 1965; Yin et al., 2015). Lamellae-shaped pores were observed in Norway spruce wood or pulp fibers infiltrated with polyethylene glycol in both the micropore and mesopore ranges, associated with aggregates of cellulose microfibrils or with cell wall checking, using atomic force microscopy and scanning electron microscopy under dry conditions (Fahlén and Salmén, 2002, 2005).

Glc infiltration prevents pore collapse and hornification, confirming that infiltration of micropores can reduce collapse associated with drying (Fahmy and Mobarak, 2008). Pores are thought to be aligned with cellulose microfibrils along with matrix molecules including lignin and hemicellulose (Salmén, 2004). Micropores may occur as water-filled spaces separating the cellulose from the matrix, as determined by wide-angle x-ray scattering (Hill et al., 2009). Micropore structures in dry wood are related to lignin, with more micropores present in hardwood than in softwood (Kojiro et al., 2010), in agreement with this study. Pores can change in size and shape during cell wall formation primarily as a result of lignification (Hafrén et al., 1999; Suzuki and Itoh, 2001), thus explaining the barrier that we observed at the S3 layer on the lumen surface, which is more highly lignified (Fig. 6, A and B).

Micropores and mesopores may be infiltrated with extractives during heartwood formation (Yin et al., 2015). Sapwood may contain more mesopores than heartwood, and this may reflect the filling of mesopores by extractives in the heartwood, resulting in a relative increase in the number of smaller micropores. This change occurred to a similar extent in earlywood and latewood (Yin et al., 2015). In this study, red beech sapwood contained significantly more extractives than radiata pine sapwood (Table 3), and this corresponded to a greater number of smaller micropores. It is unclear if this difference was due to the filling of pores with extractives or to other differences in cell wall composition.

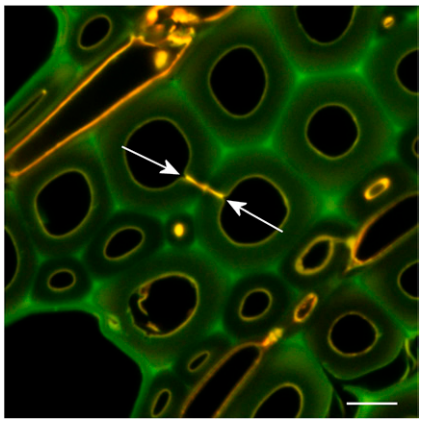

Figure 7. Fluorescence imaging of red beech heartwood. Arrows indicate the occlusion of a fiber pit pair with extractives. Autofluorescence was excited sequentially with 488 and 561 nm, with emission at 500 to 550 nm and 570 to 700 nm. Bar = 10 μm.

The extent to which water flows through xylem cell walls in living trees is poorly understood, with most water movement taking place in the lumens and pits of tracheids or vessels. Movement through cell walls may be important in cavitated xylem or in heartwood as a bypass to otherwise occluded conduits (Palin and Petty, 1981). Water stored within cell walls (30% by weight; Skaar, 1988) also might act as a reservoir for refilling cavitated xylem conduits, although this is difficult to study experimentally (Ryu et al., 2016). In beech, the occlusion of fiber pits with heartwood extractives (Fig. 7) would restrict any water movement between adjacent fibers to the cell wall micropores. The formation of tyloses in vessels and the occlusion of intervascular pits between adjacent vessels in beech also would have the same effect.

Previous attempts to measure the permeability of cell walls to water have used osmotic techniques (Palin and Petty, 1981; Petty and Palin, 1983). In spruce heartwood, the longitudinal permeability of cell walls was about 10-fold greater than that of tangential or radial permeability, and values were 1 to 2 orders of magnitude smaller than expected based on the assumption that all water is in the free state, indicating that a significant amount of water within the cell wall is in the bound state. The higher longitudinal permeability is thought to result from the orientation of pores parallel to the cellulose microfibril orientation (Preston, 1974; Donaldson and Frankland, 2004; Xu et al., 2007). Calculations based on measured permeability values indicate pore sizes in the range of 0.6 to 1.7 nm (Palin and Petty, 1981), which agrees with direct measurements (Hill and Papadopoulos, 2001; Grigsby et al., 2013). Permeability values for birch (*Betula pubescens*) and lime (*Tilia vulgaris*) are slightly smaller than those for spruce (Petty and Palin, 1983), which agrees with our findings here for beech compared with pine.

Red beech timber is very susceptible to collapse during drying (Haslett and Kininmonth, 1986; Dawson and Pearson, 2017). Our observation of cell walls with greater porosity but smaller pores in this species generally supports the involvement of micropore size in cell wall collapse. Smaller pores would generate greater tensile forces during drying and, hence, result in greater cell wall shrinkage leading to collapse (Chafe, 1987). However, this needs to be investigated for a wider range of species, including both collapse-susceptible and stable hardwood species, before a broader conclusion can be made.

Our study represents the first comparison of micropore distribution in never-dried softwood and hardwood cell walls. The distribution of micropores in tracheid and fiber cell walls in radiata pine and red beech is similar, with reduced accessibility to both quenching probes and rhodamine in the middle lamella and, to a lesser extent, in the outer secondary wall. In pine, the S1 layer is highly accessible for treated sections but not for en-bloc treatments. Accessibility of the cell wall is markedly different when comparing the infiltration of sections, where all cell wall layers are equally accessible, with en-bloc treatments, where infiltration is restricted by reduced porosity at the lumen surface in the case of rhodamine probe. Red beech has more smaller pores than does radiata pine, which may reflect differences in cell wall lignification or infiltration of micropores with extractives. In general, more lignified cell wall regions, such as the middle lamella and S3 layer, seem to be less porous, although lignification does not explain the observed reduced accessibility in the outer secondary wall of tracheids and fibers. We show that, in beech, vessel secondary walls have comparable lignification to adjacent fibers and show similar porosity. Some hardwoods are known to have more highly lignified vessel secondary walls relative to their fibers (Donaldson et al., 2001), with possible consequences for porosity and water conduction.

MATERIALS AND METHODS

Sample Preparation

Sapwood from radiata pine (*Pinus radiata*) was collected from a local sawmill, while sapwood from red beech (*Nothofagus fusca*) was collected from a tree growing in Rotorua, New Zealand. Reaction wood was avoided in both species by careful screening using microscopy. Never-dried wood samples were stored in sterile water at 4°C for 1 month while experimental work was carried out, with frequent water changes. Blocks of wood were sectioned with a sledge microtome at a thickness of 40 µm in the transverse plane, and sections were stored in water at 4°C until use. Storage of sections in the fridge was essential for beech, as sections were found to undergo significant browning at room temperature with unknown consequences for microscopic examination.

Quenching Studies

Sections of both species were treated with 0.2 µM solutions of NPGP (Sigma), NPGU (Sigma), NPXT (Megazyme), NPMP (Megazyme), and NPMH (Sigma), as well as a water control, for 1 h at room temperature (22°C) in the dark. Sections were subsequently blotted dry and allowed to air dry for 1 h before mounting in immersion oil for microscopy (Donaldson et al., 2015). Sections were examined with a Leica SP5 II confocal microscope using 355-nm excitation and 400- to 550-nm emission under conditions for low-intensity illumination to avoid UV-induced photodegradation (30-mW laser power, 10% acoustooptical tunable filter, 3× line accumulation, 4× frame averaging, pinhole 2 Airy units, 63× 1.4 numerical aperture objective, 3× digital zoom, 12-bit dynamic range: 0–4,096 gray levels). For quantitative measurement of nitrophenol-induced quenching of lignin fluorescence, 10 fields of view were examined for each probe.

Images were analyzed for average cell wall fluorescence intensity with a threshold of 150 gray levels to differentiate cell walls from lumens using Digital Optics V++ software. Both the total cell wall brightness and the brightness of the secondary wall and middle lamella for tracheids and fibers were measured. Cell wall layers were detected by differential segmentation using a threshold of 55% of the average cell wall brightness (Moëll and Donaldson, 2001). Quenching relative to a water-treated control was calculated by Equation 1:

$$Q = (A-B)/A$$

where A is the intensity of the control and B is the intensity of the quenched sample.

Rhodamine Infiltration and FRET

Sections were treated with a 1.6 µM solution of rhodamine B (BDH) for 1 h in the dark at room temperature. Sections were mounted in either 50% (v/v) glycerol in phosphate buffer at pH 7, or in immersion oil after air drying for 1 h, and examined by confocal fluorescence microscopy using sequential excitation at 458 and 561 nm and emission at 470 to 560 nm (lignin) and 570 to 700 nm (rhodamine). Sections without rhodamine staining were used as controls and were imaged at the same gain setting as the rhodamine-treated sections. FRET measurements were performed by acceptor photobleaching with bleaching carried out at 561 nm with 100% laser power for 50 scans on a rectangular region of interest (Donaldson et al., 2014). Five fields of view were examined for each treatment.

In addition to the treatment of sections, water-saturated and air-dried blocks of pine and beech with microtomed transverse ends, approximately 5 mm × 5 mm × 2 cm, were treated with rhodamine solution for 24 h in the dark and sectioned subsequently for microscopy. Blocks were sectioned longitudinally in the radial plane to measure the distance of rhodamine penetration of cell walls from the cut transverse and longitudinal faces and again in the transverse plane behind the zone of rhodamine infiltration. Unstained controls also were examined. FRET measurements on en-bloc samples were performed in immersion oil to reduce the possibility of rhodamine becoming mobile during microscopy.

Chemical Analysis

Samples of pine and beech were analyzed to determine their lignin and carbohydrate composition. The pine sample was extracted using dichloromethane solvent on a Soxtec apparatus, with a boiling time of 0.5 h and a rinse time of 1 h. The beech sample was extracted using methanol on a Soxtec apparatus, with a boiling time of 1 h and a rinse time of 1 h. Acid-insoluble lignin was determined using a modified method based on the Technical Association of the Pulp and Paper Industry Standard Methods, T 222 om-88 (Kerr, 1976). Acid-soluble lignin was determined using a modified Technical Association of the Pulp and Paper Industry Method UM 250. Carbohydrates were determined using a modified wood sugar analysis by anion chromatography (Pettersen and Schwandt, 1991).

Solutions of quenching agents and rhodamine as used for microscopy but with 10-fold dilution and filtration through a 0.45-µm membrane filter were examined by dynamic light scattering to determine their Stokes radius. Dynamic light-scattering measurements were made with a Malvern Zetasizer Nano ZS (Malvern Instruments). The instrument was fitted with a 633-nm laser source and operated in a backscatter geometry (173°), with the sample temperature controlled at 25°C ± 0.1°C. The results are reported as averages of triplicate measurements. Each measurement consisted of a number of submeasurements of 10 s duration, with total measurement duration optimized by the software on a per-sample basis, usually 100 to 150 s. The measured light

scattering was modeled by the instrument software in one of two ways: (1) Z-average particle diameter and polydispersity were obtained by modeling the correlation data with a single decay curve; and (2) size distribution data were obtained by fitting the measured correlation data with theoretical correlation curves generated for 70 size brackets for particles between 0.4 and 1,000 nm in diameter. Two different theoretical size distributions were calculated: one suitable for polydisperse samples and one weighted toward multiple narrow size distributions.

Molecular models of quenching probes and rhodamine were structurally minimized with modified Allinger force field (MM2) parameters using Chem3DPro version 12 (CambridgeSoft). Molecular dynamics were then performed on the initially minimized structures followed by further MM2 minimizations. This process was repeated until energy minimums were achieved. The water-accessible surface, set at 1.4 Å, was calculated by an extended Hückel semiempirical method. It was assumed that the quenching probe and rhodamine molecules remained hydrated under the conditions used and presented a major molecular interaction with lignin determined by their distribution within the cell wall.

Histochemistry

For the measurement of cell wall lignin concentration, small 2- × 3-mm blocks of radiata pine and red beech were dehydrated in acetone and embedded in Spurr resin. Transverse sections 2 µm in thickness were cut with a glass knife and heat fixed to microscope slides at 70°C. Sections were treated with sodium ethoxide for 5 min at room temperature to remove the embedding resin. Refractive index measurements and calculation of lignin percentage (v/v) were performed using interference microscopy as described by Donaldson (1992). Measurements were performed on each of 10 cells. For radiata pine, the S2 and middle lamella regions of the cell wall were measured, whereas for red beech, the S2 regions of fibers and vessels and the middle lamella region of fibers were measured.

For the immunolocalization of mannan and xylan, small 2- × 3-mm blocks of radiata pine and red beech were dehydrated in ethanol and embedded in LR White resin. Transverse sections 700 nm in thickness were cut with a diamond knife and allowed to air dry onto silane-coated microscope slides at room temperature. Sections were blocked to reduce nonspecific labeling using 10 mM phosphate-buffered saline containing 1% (w/v) acetylated bovine serum albumin and 50 mM Gly for 1 h at room temperature. Sections were immunolabeled with LM11 (anti-xylan) and LM21 (anti-mannan) antibodies (Plant Probes) for 2 h at room temperature (Donaldson and Knox, 2012). Primary antibody labeling was localized using goat anti-rat secondary antibody labeled with Alexa 633 (Life Technologies). Sections were mounted in Citifluor antifade oil and imaged using confocal fluorescence with excitation at 633 nm and emission at 650 to 790 nm. Similar sections were stained with 0.001% (w/v) acriflavin for 5 min to localize lignin. In this case, excitation was at 476 nm and emission was at 490 to 600 nm. To determine cell wall layering, sections were examined in wide-field transmission using polarized light.

Statistical Analyses

ANOVA was used to determine 95% confidence intervals for quenching and FRET measurements and for chemistry and histochemistry measurements.

ACKNOWLEDGMENTS

We thank Bernadette Nanayakkara, Andrew Vogt, Warren Grigsby, Hamish Pearson, and Elspeth MacRae (Scion) for their comments on the article as well as Sunita Jeram and Katrina Martin (Scion) for performing the chemical analysis of wood samples. Hamish Pearson (Scion) provided the sample of red beech wood.

Received July 17, 2018; accepted September 6, 2018; published September 14, 2018.

LITERATURE CITED

Blanchette RA, Krueger EW, Haight JE, Akhtar M, Akin DE (1997) Cell wall alterations in loblolly pine wood decayed by the white-rot fungus, *Ceriporiopsis subvermispora*. J Biotechnol **53**: 203–213

Borrega M, Kärenlampi PP (2011) Cell wall porosity in Norway spruce wood as affected by high-temperature drying. Wood Fiber Sci **43**: 206–214

Brodersen CR, McElrone AJ (2013) Maintenance of xylem network transport capacity: a review of embolism repair in vascular plants. Front Plant Sci **4**: 108

Chafe SC (1987) Collapse, volumetric shrinkage, specific gravity and extractives in *Eucalyptus* and other species. Wood Sci Technol **21**: 27–41

Choat B, Cobb AR, Jansen S (2008) Structure and function of bordered pits: new discoveries and impacts on whole-plant hydraulic function. New Phytol **177**: 608–625

Chundawat SPS, Donohoe BS, da Costa Sousa L, Elder T, Agarwal UP, Lu F, Ralph J, Himmel ME, Balanab V, Dale BE (2011) Multi-scale visualisation and characterization of lignocellulosic plant cell wall deconstruction during thermochemical pretreatment. Energy Environ Sci **4**: 973–984

Ciesielski PN, Matthews JF, Tucker MP, Beckham GT, Crowley MF, Himmel ME, Donohoe BS (2013) 3D electron tomography of pretreated biomass informs atomic modeling of cellulose microfibrils. ACS Nano **7**: 8011–8019

Davies GW (1968) Electron microscopy and cell wall porosity. Appita **21**: 117–130

Dawson BSW, Pearson H (2017) Effect of supercritical CO_2 dewatering followed by oven-drying of softwood and hardwood timbers. Wood Sci Technol **51**: 771–784

Donaldson LA (1987) S3 lignin concentration in radiata pine tracheids. Wood Sci Technol **21**: 227–234

Donaldson LA (1988) Ultrastructure of wood cellulose substrates during enzymatic hydrolysis. Wood Sci Technol **22**: 33–41

Donaldson LA (1992) Interference microscopy. *In* **SY Lin, CW Dence**, eds, Methods in Lignin Chemistry. Springer Verlag, Berlin, pp 122–132

Donaldson LA (1995) Cell wall fracture properties in relation to lignin distribution and cell dimensions among three genetic groups of radiata pine. Wood Sci Technol **29**: 51–63

Donaldson LA (2001) Lignification and lignin topochemistry: an ultrastructural view. Phytochemistry **57**: 859–873

Donaldson LA, Frankland A (2004) Ultrastructure of iodine treated wood. Holzforschung **58**: 219–225

Donaldson LA, Knox JP (2012) Localization of cell wall polysaccharides in normal and compression wood of radiata pine: relationships with lignification and microfibril orientation. Plant Physiol **158**: 642–653

Donaldson LA, Vaidya A (2017) Visualising recalcitrance by colocalisation of cellulase, lignin and cellulose in pretreated pine biomass using fluorescence microscopy. Sci Rep **7**: 44386

Donaldson LA, Hague JRB, Snell R (2001) Lignin distribution in coppice poplar, linseed and wheat straw. Holzforschung **55**: 379–385

Donaldson LA, Newman RH, Vaidya A (2014) Nanoscale interactions of polyethylene glycol with thermo-mechanically pre-treated *Pinus radiata* biofuel substrate. Biotechnol Bioeng **111**: 719–725

Donaldson LA, Kroese HW, Hill SJ, Franich RA (2015) Detection of wood cell wall porosity using small carbohydrate molecules and confocal fluorescence microscopy. J Microsc **259**: 228–236

Fahlén J, Salmén L (2002) On the lamellar structure of the tracheid cell wall. Plant Biol **4**: 339–345

Fahlén J, Salmén L (2005) Pore and matrix distribution in the fiber wall revealed by atomic force microscopy and image analysis. Biomacromolecules **6**: 433–438

Fahmy TYA, Mobarak F (2008) Vaccination of biological cellulose fibers with glucose: a gateway to novel nanocomposites. Int J Biol Macromol **42**: 52–54

Grigsby WJ, Kroese H, Dunningham EA (2013) Characterisation of pore size distribution in variously dried *Pinus radiata*: analysis by thermoporosimetry. Wood Sci Technol **47**: 737–747

Hacke UG, Sperry JS (2001) Functional and ecological xylem anatomy. Perspect Plant Ecol Evol Syst **4**: 97–116

Hafrén J, Fujino T, Itoh T (1999) Changes in cell wall architecture of differentiating tracheids of *Pinus thunbergia* during lignification. Plant Cell Physiol **40**: 532–541

Haslett AN, Kininmonth JA (1986) Pretreatments to hasten the drying of *Nothofagus fusca*. N Z J For Sci **16**: 237–246

Hill CAS, Papadopoulos AN (2001) A review of methods used to determine the size of the cell wall microvoids of wood. J Inst Wood Sci **15**: 337–345

Hill CAS, Forster SC, Farahani MRM, Hale MDC, Ormondroyd GA, Williams GR (2005) An investigation of cell wall micropore blocking as a possible mechanism for the decay resistance of anhydride modified wood. Int Biodet Biodeg **55**: 69–76

Hill SJ, Franich RA, Callaghan PT, Newman RH (2009) Nature's nanocomposite: a new look at molecular architecture in wood cell walls. N Z J For Sci **39**: 251–257

Kerr AJ (1976) Ash, silica, and lignin in New Zealand beech. N Z J For Sci **6**: 108–113

Kielmann BC, Adamopoulos S, Militz H, Koch G, Mai C (2014) Modification of three hardwoods with an N-methylol melamine compound and a metal-complex dye. Wood Sci Technol **48**: 123–136

Kim JS, Daniel G (2012a) Distribution of glucomannans and xylans in poplar xylem and their changes under tension stress. Planta **236**: 35–50

Kim JS, Daniel G (2012b) Immunolocalization of hemicelluloses in Arabidopsis thaliana stem. Part II. Mannan deposition is regulated by phase of development and its patterns of temporal and spatial distribution differ between cell types. Planta **236**: 1367–1379

Kishi K, Harada H, Saiki H (1977) Layered structure of the secondary wall in vessels of hardwoods by polarizing microscopy. Bull Kyoto Univ For **49**: 122–126

Kobayashi T, Sakai Y, Iizuka K (1960) Hydrolysis of cellulose in a small amount of concentrated sulfuric acid. Bull Agric Chem Soc Jpn **24**: 443–449

Kojiro K, Miki T, Sugimoto H, Nakajima M, Kanayama K (2010) Micropores and mesopores in the cell wall of dry wood. J Wood Sci **56**: 107–111

McCully M, Canny M, Baker A, Miller C (2014) Some properties of the walls of metaxylem vessels of maize roots, including tests of the wettability of their lumenal wall surfaces. Ann Bot **113**: 977–989

Meng Y, Xia Y, Young TM, Cai Z, Wang S (2015) Viscoelasticity of wood cell walls with different moisture content as measured by nanoindentation. RSC Advances **5**: 47538–47547

Moëll M, Donaldson LA (2001) Comparison of segmentation methods for digital image analysis of confocal microscope images to measure tracheid cell dimensions. IAWA J **22**: 267–288

Palin MA, Petty JA (1981) Permeability to water of the cell wall material of spruce heartwood. Wood Sci Technol **15**: 161–169

Pettersen RC (1991) Wood sugar analysis by anion chromatography. J Wood Chem Technol **11**: 495–501

Pettersen RC, Schwandt VH (1991) Wood sugar analysis by anion chromatography. J Wood Chem Technol **11**: 495–501

Petty JA, Palin MA (1983) Permeability to water of the fibre cell wall material of two hardwoods. J Exp Bot **34**: 688–693

Preston RD (1974) The Physical Biology of Plant Cell Walls. Chapman and Hall, London

Pu Y, Hu F, Huang F, Davison BH, Ragauskas AJ (2013) Assessing the molecular structure basis for biomass recalcitrance during dilute acid and hydrothermal pretreatments. Biotechnol Biofuels **6**: 15

Rouquerol J, Avnir D, Fairbridge CW, Everett DH, Haynes JH, Pernicone N, Ramsay JDF, Sing KSW, Unger KK (1994) Recommendations for the characterization of porous solids (technical report). Pure Appl Chem **66**: 1739–1758

Ryu J, Hwang BG, Lee SJ (2016) In vivo dynamic analysis of water refilling in embolized xylem vessels of intact Zea mays leaves. Ann Bot **118**: 1033–1042

Salmén L (2004) Micromechanical understanding of the cell-wall structure. C R Biol **327**: 873–880

Sannigrahi P, Kim DH, Jung S, Ragauskas A (2011) Pseudo-lignin and pretreatment chemistry. Energy Environ Sci **4**: 1306–1310

Scheller HV, Ulvskov P (2010) Hemicelluloses. Annu Rev Plant Biol **61**: 263–289

Schönherr J (2006) Characterization of aqueous pores in plant cuticles and permeation of ionic solutes. J Exp Bot **57**: 2471–2491

Skaar C (1988) Wood-Water Relations. Springer, Berlin

Sorieul M, Dickson A, Hill SJ, Pearson H (2016) Plant fibre: molecular structure and biomechanical properties, of a complex living material, influencing its deconstruction towards a biobased composite. Materials (Basel) **9**: 618

Stone JE (1964) The porous structure of wood and fibres. Pulp Paper Mag Can **65**: T3–T13

Stone JE, Scallan AM (1965) Effect of component removal upon the porous structure of the cell wall of wood. J Polym Sci **11**: 13–25

Suzuki K, Itoh T (2001) The changes in cell wall architecture during lignification of bamboo, *Phyllostachys aurea* Carr. Trees (Berl) **15**: 137–147

Wu N, Hubbe MA, Rojas OJ, Park S (2009) Permeation of polyelectrolytes and other solutes into the pore spaces of water-swollen cellulose: a review. BioResources **4**: 1222–1262

Wu X, Lin J, Lin Q, Wang J, Schreiber L (2005) Casparian strips in needles are more solute permeable than endodermal transport barriers in roots of *Pinus bungeana*. Plant Cell Physiol **46**: 1799–1808

Xu P, Donaldson LA, Gergely ZR, Staehelin LA (2007) Dual-axis electron tomography: a new approach for investigating the spatial organisation of wood cellulose microfibrils. Wood Sci Technol **41**: 101–116

Yin J, Song K, Lu Y, Zhao G, Yin Y (2015) Comparison of changes in micropores and mesopores in the wood cell walls of sapwood and heartwood. Wood Sci Technol **49**: 987–1001

Yin J, Yuan T, Lu Y, Song K, Li H, Zhao G, Yin Y (2017) Effect of compression combined with steam treatment on the porosity, chemical composition and cellulose crystalline structure of wood cell walls. Carbohydr Polym **155**: 163–172

Zwieniecki MA, Holbrook NM (2000) Bordered pit structure and vessel wall surface properties: implications for embolism repair. Plant Physiol **123**: 1015–1020